



# Li<sup>+</sup> Cations Activate NiFeOOH for Oxygen Evolution in Sodium and Potassium Hydroxide

Onno van der Heijden, Jordy J. J. Eggebeen, Hanna Trzesniowski, Nipon Deka, Ronny Golnak, Jie Xiao, Maartje van Rijn, Rik V. Mom, and Marc T. M. Koper\*

**Abstract:** The efficiency of electrolysis is reduced due to the sluggish oxygen evolution reaction (OER). Besides catalyst properties, electrocatalytic activity also depends on the interaction of the electrocatalyst with the electrolyte. Here, we show that the addition of small amounts of Li<sup>+</sup> to Fe-free NaOH or KOH electrolytes activates NiFeOOH for the OER compared to single-cation electrolytes. Moreover, the activation was maintained when the solution was returned to pure NaOH. Importantly, we show that the origin of activation by Li<sup>+</sup> cations is primarily non-kinetic in nature, as the OER onset for the mixed electrolyte does not change and the Tafel slope at low current density is ~30 mV/dec in both electrolytes. However, the increase of the apparent Tafel slope remains lower at increasing current densities in the presence of Li<sup>+</sup>. Based on electrochemical quartz crystal microbalance and in situ X-ray absorption spectroscopy measurements, we show that this reduction of non-kinetic effects is due to enhanced intercalation of sodium, water and hydroxide. This enhanced electrolyte penetration facilitates the OER, especially at higher current densities and for increased catalyst loading. Our work shows that mixed electrolytes where distinct cations can have different roles provide a simple and promising strategy towards improved OER rates.

## Introduction

Hydrogen production through alkaline water electrolysis has been a mature industrial-scale process for many decades. Despite its maturity, the technology remains relatively energy inefficient, which is a major bottleneck for the energy transition in the chemical industry, which will require vast volumes of green hydrogen as a feedstock. The efficiency of water splitting is limited by the kinetically sluggish oxygen evolution reaction (OER), which is the complementary reaction to hydrogen evolution. Under alkaline conditions, Ni<sub>1-x</sub>Fe<sub>x</sub>OOH has been reported as one of the most active catalysts for the oxygen evolution reaction,<sup>[1]</sup> both as synthesised catalyst or as the in situ phase formed for any nickel-based catalyst in an electrolyte that has not been made iron free. These catalysts are layered double hydroxides (LDH), in which the oxyhydroxide phase has intercalated cations, anions and water in between the oxyhydroxide layers.<sup>[2]</sup> To improve electrocatalytic performance, many different catalyst compositions and morphologies have been investigated.<sup>[3]</sup> However, in addition to the catalyst properties, the optimization of the electrolyte is a promising but understudied route to improve OER activity. Electrolyte properties such as pH,<sup>[4]</sup> iron impurities<sup>[5]</sup> and the choice of cation have a marked effect on the observed OER activity. Interestingly, when these parameters are combined, the effect on the activity is not additive, but rather follows a poorly understood pattern. For example, in Fe-free electrolyte, the cation-dependent activity trend is CsOH > KOH ≈ NaOH > LiOH,<sup>[6]</sup> whereas in Fe-saturated electrolyte the trend is KOH ≈ NaOH > CsOH > LiOH.<sup>[5a]</sup> This highlights the need for a better understanding of the origin of electrolyte effects to fully exploit them.

Another enigmatic, but promising direction for tuning electrolyte properties is the use of mixed electrolytes containing multiple species. For instance, a mixed electrolyte with NaCl has shown to improve electrolyte “break-in” at moderate pH, which improves the activity.<sup>[7]</sup> Although studies on mixed electrolytes are scarce, some interesting observations were also made for NiFe batteries, which also use nickel oxyhydroxide (NiOOH) electrodes. In NiFe batteries, electrolyte cations intercalate into the oxyhydroxide upon charging and are expelled upon discharging.<sup>[8]</sup> It has been found that the addition of LiOH to the KOH electrolyte improves the capacity of these NiFe batteries,<sup>[9]</sup> as well as their coulombic efficiency.<sup>[10]</sup> Furthermore, the addition of LiOH to the electrolyte results in an improvement in the reversibility of the Ni redox peaks.<sup>[11]</sup> The

[\*] O. van der Heijden, J. J. J. Eggebeen, N. Deka, M. van Rijn, R. V. Mom, M. T. M. Koper  
 Leiden Institute of Chemistry, Leiden University, Einsteinweg 55, 2333 CC, Leiden, the Netherlands  
 E-mail: m.koper@chem.leidenuniv.nl

H. Trzesniowski  
 Department of Atomic-Scale Dynamics in Light-Energy Conversion, Helmholtz-Zentrum Berlin für Materialien und Energie, Albert-Einstein-Straße 15, 12489 Berlin, Germany

R. Golnak, J. Xiao  
 Department of Highly Sensitive X-Ray Spectroscopy, Helmholtz-Zentrum Berlin für Materialien und Energie, 14109 Berlin, Germany

© 2024 The Authors. Angewandte Chemie International Edition published by Wiley-VCH GmbH. This is an open access article under the terms of the Creative Commons Attribution License, which permits use, distribution and reproduction in any medium, provided the original work is properly cited.

improved reversibility of the Ni redox peaks has been related to more facile interlayer hydroxide diffusion.<sup>[12]</sup> For the so-called battolyser setup, which is a combination of a NiFe battery and a water electrolyzer in a single system, the overall cell potential was found to be lower with a 6.45 M KOH electrolyte mixed with 0.05 M LiOH, compared to 6.5 M KOH.<sup>[11]</sup> However, the exact nature of these mixed-electrolyte effects is not yet understood.

To capture the origin of the Li<sup>+</sup>-promotion in mixed electrolytes and harness it for the OER, we studied the effect of mixing small amounts of LiOH with (Fe-free) NaOH and KOH electrolytes for the OER on NiFeOOH at a constant bulk pH. We observed that the addition of LiOH resulted in significantly increased activity. More specifically, the addition of Li<sup>+</sup> reduced the non-kinetic contribution to the OER overpotential as evidenced by the mitigation of the increase in apparent Tafel slope values at increasing current densities. Using electrochemical quartz crystal microbalance (eQCM) and X-ray absorption spectroscopy (XAS), the improved activity can be related to increased mass intercalation into the porous catalyst layer. This increase is due to a more pronounced sodium and water/hydroxide uptake in the porous catalyst layer in the presence of a small amount of Li<sup>+</sup>. This increased electrolyte penetration results in more accessible redox-active sites, as shown by a more pronounced Ni<sup>4+</sup> signal at relevant OER potentials. Our work shows how the optimization of the electrolyte-electrode interface is a promising approach to improve electrocatalytic performance of a given electrocatalyst, and how for OER this optimization is dictated by the accessibility of the porous catalyst. This research opens new strategies wherein distinct cations can have different roles to optimize electrocatalytic performance.

## Results and discussion

Figure 1A shows the CVs of NiFeOOH in 0.1 M XOH (LiOH, NaOH, KOH and CsOH), for an electrodeposited catalyst (Ni<sub>80</sub>Fe<sub>20</sub>OOH) produced with the following cathodic electrodeposition conditions: 5 s at  $-8$  mA per cm<sup>2</sup> per real gold surface area ( $-8$  mA/cm<sup>2</sup><sub>Au</sub>). The cathodic deposition conditions used here are similar to those previously

reported for this common OER catalyst.<sup>[13]</sup> Under the applied anodic potential the material will reconstruct into  $\gamma$ -NiFeOOH,<sup>[14]</sup> similar to Co(Fe)OOH.<sup>[15]</sup> The mass increase during the deposition of the catalyst layer was followed with eQCM (Figure S1) and the resulting morphology of the catalyst layer was analysed with SEM (Figure S2). Moreover, ICP-MS was used to confirm that the final catalyst layer indeed contained approximately 80 % nickel and 20 % iron (Supporting Information Table 1). To confirm that the electrolytes are sufficiently iron free, NiOOH was electrodeposited and cycled in the electrolyte to check for (lack of) iron contamination, as shown in Figure S3. The data show that in Fe-free 0.1 M XOH electrolyte, the activity follows the order of Cs > K  $\approx$  Na > Li (Figure 1A), as reported previously.<sup>[6]</sup> The reason for this cation effect is still under debate. It has been hypothesized to be caused by local cation/OH<sup>-</sup> concentration,<sup>[6b]</sup> by differences in bulk pH<sup>[16]</sup> or by a direct promotion of the active site.<sup>[6a]</sup> To ensure the effect measured here is not due to differences in bulk pH, the solutions were carefully prepared by controlling the pH. The pH was measured by titration (Supporting Information Table 2) because the pH of LiOH cannot be measured accurately using a glass pH meter.<sup>[16]</sup> Furthermore, day-to-day changes were avoided by performing measurements on the same day on the same setup with freshly electrodeposited NiFeOOH catalysts for each electrolyte.

When LiOH, the least active single-cation electrolyte, was mixed in small amounts with NaOH (10 mM LiOH, 90 mM NaOH), the activity increased while the pH was constant (Figure 1B). Furthermore, LiOH added to KOH, again for a total of 0.1 M XOH, has a similar effect (Figure 1C). The optimum Li<sup>+</sup> concentration was determined to be at  $\sim$ 10 mM LiOH (Figure S4). Besides the improved activity, the nickel oxidation occurs slightly faster (as shown by a faster initial increase in current), while the nickel reduction peak does not change significantly. The differences in Ni oxidation behaviour were more pronounced at increasing scan rate, which shows the reduced limitation for Ni oxidation in Na<sub>90</sub>Li<sub>10</sub>OH compared to NaOH (Figures S5 and S6). Differences in the nickel oxidation peak potential were also observed in pure LiOH, NaOH, KOH and CsOH (Figure 1A) and for different pH, as also observed in earlier research.<sup>[11, 12]</sup> Interestingly, the

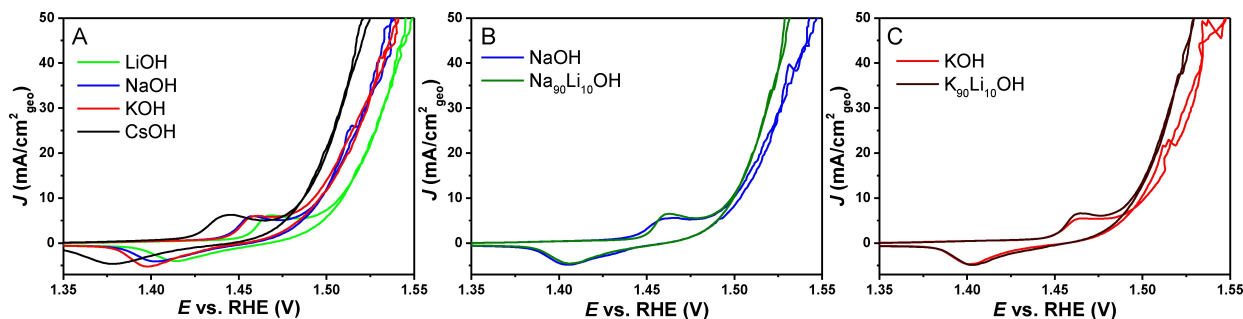


**Figure 1.** (A) CVs of freshly deposited NiFeOOH in 0.1 M LiOH, NaOH, KOH and CsOH, (B) CVs of freshly electrodeposited NiFeOOH layers measured in 0.1 M NaOH and 0.1 M Na<sub>90</sub>Li<sub>10</sub>OH, (C) CVs of freshly electrodeposited NiFeOOH layers measured in 0.1 M KOH and 0.1 M K<sub>90</sub>Li<sub>10</sub>OH. All CVs were recorded at 10 mV/s, 2500 RPM and 100% iR corrected (85% in situ, 15% manually afterwards).

addition of LiOH to CsOH does not seem to have the same effect as observed for NaOH and KOH (Figure S7).

To study if this Li<sup>+</sup> promotion effect applies over a wider pH range, experiments were performed in both 0.05 M and 0.5 M XOH showing that the Li<sup>+</sup> promotion effect is still observed at the same Li<sup>+</sup> concentration of 10 mM Li<sup>+</sup> (Figure S8). Moreover, the activity in pure NaOH was maintained after Li<sup>+</sup> activation and was similar to that in Na<sub>90</sub>Li<sub>10</sub>OH (Figure S9). The (semi-)permanent change of the Li<sup>+</sup> activation was also found in the battolyser, where the effect was observed up to 30 cycles after switching back from 6.45 M KOH + 0.05 M LiOH to 6.5 M KOH.<sup>[11]</sup> This non-reversibility presents the opportunity for pre-activation treatments, although the long-term stability without LiOH in the electrolyte has not been evaluated here. Improved activity was also observed after switching electrolytes from NaOH to Na<sub>90</sub>Li<sub>10</sub>OH using the same catalyst layer (Figure S10), demonstrating that the Li<sup>+</sup> promotion effect is robust and reproducible. Moreover, LSVs were taken on a high speed RDE at 4000 RPM to higher current density, showing the robustness of the Li activation effect up to 250 mA/cm<sup>2</sup><sub>geo</sub> and during 3 minutes of chronopotentiometry (CP) at 100 mA/cm<sup>2</sup><sub>geo</sub>, which confirms that the activity enhancement is not due to the dynamic nature of CVs or LSVs (Figure S11).

Insight into the exact nature of the Li<sup>+</sup> activation effect can be obtained from the Tafel slope values at low current densities before non-kinetic effects have a large effect,<sup>[17]</sup> as well as from the onset of OER activity. To extract the Tafel slope at low current densities, the majority of the Ni oxidation contribution was removed by a CV-CA-LSV program. In this approach, a CV is recorded to a potential just positive of the Ni oxidation peak (1.525 V vs. RHE) and scanned back to a potential just prior to nickel reduction (1.455 V vs. RHE), next a CA is performed at that potential for 10 s (1.455 V vs. RHE) after which a LSV is taken into the OER potential region (the procedure is provided in

Figure S12). In Figure 2A, the LSV shows a similar activity at low current density (<2 mA/cm<sup>2</sup><sub>geo</sub>) in both electrolytes and from this LSV the Tafel slopes were computed over small intervals (20 mV). The Tafel slopes were then plotted vs. the average current density, as shown in Figure 2B. In this Figure, it can be observed that at low current densities the Tafel slope value is ~30 mV/dec, similar to KOH,<sup>[17]</sup> for both NaOH and Na<sub>90</sub>Li<sub>10</sub>OH. However, the increase in (apparent) Tafel slope was strongly reduced with Li<sup>+</sup> in solution. This increase in (apparent) Tafel slope has previously been related to non-kinetic effects, such as bubble formation and mass transport effects inside the catalyst<sup>[17]</sup> or in the external electrolyte.<sup>[18]</sup> Internal mass transport effects are more likely here than bubble formation, as bubble formation and release for both electrolytes at constant current are quite similar (Figure S13). The onset of the OER and the Tafel slope of ~30 mV/dec at low current density do not change significantly between the electrolytes. Therefore, Figure 2 strongly suggests that the addition of small amounts of Li<sup>+</sup> does not have an intrinsic effect on the OER kinetics, such as a change in Tafel slope value due to a different rate-determining step or an earlier onset due to changes in the energetics of the reaction intermediates. Rather, it helps to mitigate the non-kinetic limitations at increasing current densities. We emphasize that there is currently no simple model that can explain Tafel slope behaviour shown in Figure 2B, though it is clear that mass transport effects that are difficult to remove play an important role.

To further investigate the nature of the ion-electrode interactions, eQCM measurements were performed. Ni-FeOOH takes up mass via intercalation during the oxidation of nickel and expels mass during reduction.<sup>[2d,19]</sup> An increase in mass in eQCM is shown as a decrease in  $\Delta$ frequency. This mass increase is strongly dependent on the cation identity and scales with the cation molar mass, as is shown in Figure S16. Interestingly, the total intercalated mass is larger

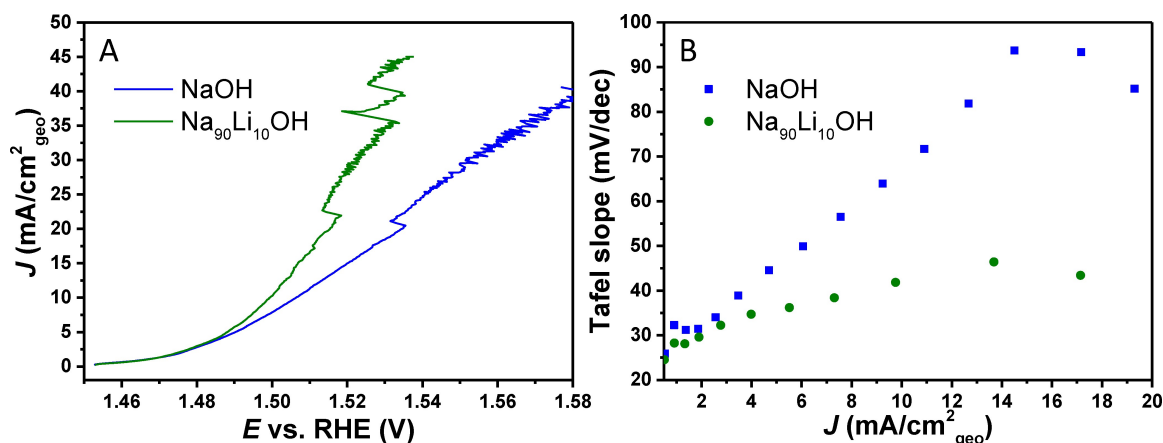


**Figure 2.** (A) 100% iR corrected LSV measured at 5 mV/s and 2500 RPM with reduced Ni oxidation contribution (bubble releases combined with iR correction cause the spike features in the LSV), (B) corresponding Tafel slope behaviour, computed over 20 mV intervals and plotted vs. the average current between 0 and 20 mA/cm<sup>2</sup><sub>geo</sub>. The increase in the apparent Tafel slope is strongly reduced in the mixed electrolyte, but initially it is ~30 mV/dec for both electrolytes. Zoomed-in LSVs on the low current density region and corresponding Tafel slope values are shown in Figure S14 and a similar plot but for KOH and K<sub>90</sub>Li<sub>10</sub>OH is shown in Figure S15.

in 0.1 M  $\text{Na}_{90}\text{Li}_{10}\text{OH}$  compared to 0.1 M NaOH (Figure 3), even though the average cation mass has decreased when 10% of the  $\text{Na}^+$  has been replaced with  $\text{Li}^+$ . Hence, the presence of LiOH in the solution results in enhanced mass intercalation within the layered  $\text{NiFeOOH}$  structure. Although, the  $\text{NiFeOOH}$  LDH layer might not be rigid enough for the Sauerbrey equation to be valid for determining the precise mass change,<sup>[20]</sup> the relative mass change can still be qualitatively compared when assuming both layers will have a similar rigidity. Furthermore, the contribution of specific species cannot be disentangled with eQCM, for example, carbonate species that are likely present in the LDH could also be intercalated or expelled upon Ni reduction or oxidation. However, the most reasonable explanation for the observation in Figure 3 is that the presence of  $\text{Li}^+$  enhances the intercalation of  $\text{Na}^+$  as the mass increase scales with the cation molar mass for the pure electrolytes and  $\text{Li}^+$  has a low mass (Figure S16).

To elucidate which species are intercalating into the porous catalyst layer, and what further implications this has for the catalyst electronic structure and local environment, in situ XAS was performed at the Na K-edge, O K-edge and Ni L-edge. As shown in previous work, the spectral features of the Na K-edge can be used to dynamically track the sodium intercalation into the catalyst. Furthermore, in agreement with previous measurements, we see a fair amount of intercalated sodium prior to nickel oxidation (e.g. at 1.0 V).<sup>[21]</sup> Figure S17 shows that the sodium signal tracks the nickel oxidation and reduction features, similar to what is observed for the eQCM measurements, thus linking the mass change observed in eQCM to  $\text{Na}^+$  intercalation observed by XAS.<sup>[21]</sup> Important to note is that the XAS signal at the start and end of the potential cycle have the exact same value (similar to eQCM). This shows that the beamline was sufficiently stable to compare the absolute

XAS signals between different spectra, as we will do in the analysis below.

To confirm that the increase in mass intercalation in 0.1 M  $\text{Na}_{90}\text{Li}_{10}\text{OH}$  is also caused (at least in part) by  $\text{Na}^+$ , the sodium K-edge spectra in the different electrolytes were compared at 1.0, 1.45 and 1.7 V (not iR corrected). First 0.1 M NaOH was used, after which the electrolyte was switched to 0.1 M  $\text{Na}_{90}\text{Li}_{10}\text{OH}$ , upon which it was returned to 0.1 M NaOH again. The spectra (Figure 4) show that in  $\text{Na}_{90}\text{Li}_{10}\text{OH}$  there is an increased uptake of sodium cations within the porous catalyst layer, even though there is 10% less  $\text{Na}^+$  in solution. The increased sodium uptake is in agreement with the eQCM measurements shown in Figure 3, and confirms that  $\text{Na}^+$  intercalation is boosted by the presence of small amounts of  $\text{Li}^+$  in the electrolyte. This increase in the  $\text{Na}^+$  signal is observed for all measured potentials. When the electrolyte was changed back to NaOH, the increase in  $\text{Na}^+$  uptake is observed to be maintained, in agreement with the non-reversible increase in OER rate seen after treatment in 0.1 M  $\text{Na}_{90}\text{Li}_{10}\text{OH}$  (Figure S9). This non-reversible increase in activity was indeed reproduced during the in situ XAS experiment, as shown Figure S18. When the electrolyte was returned to pure NaOH the sodium signal is slightly higher compared to  $\text{Na}_{90}\text{Li}_{10}\text{OH}$ , probably as there is more  $\text{Na}^+$  in solution, and the  $\text{Li}^+$  induced change in the catalyst was maintained.

Complementing the Na K-edge data, the oxygen K-edge was measured. This signal allows us to probe the lattice oxygen species of the  $\text{NiFeO}_x$  as well as water and/or  $\text{OH}^-$  present in the porous catalyst layer. Note that the water and hydroxide signals cannot be disentangled, although water is expected to be present in much higher concentration. In Figure 5, the intensity of the water/hydroxide peak (535–545 eV) is observed to increase for  $\text{Na}_{90}\text{Li}_{10}\text{OH}$ , showing the more pronounced presence of  $\text{H}_2\text{O}$  and  $\text{OH}^-$  in the catalyst.

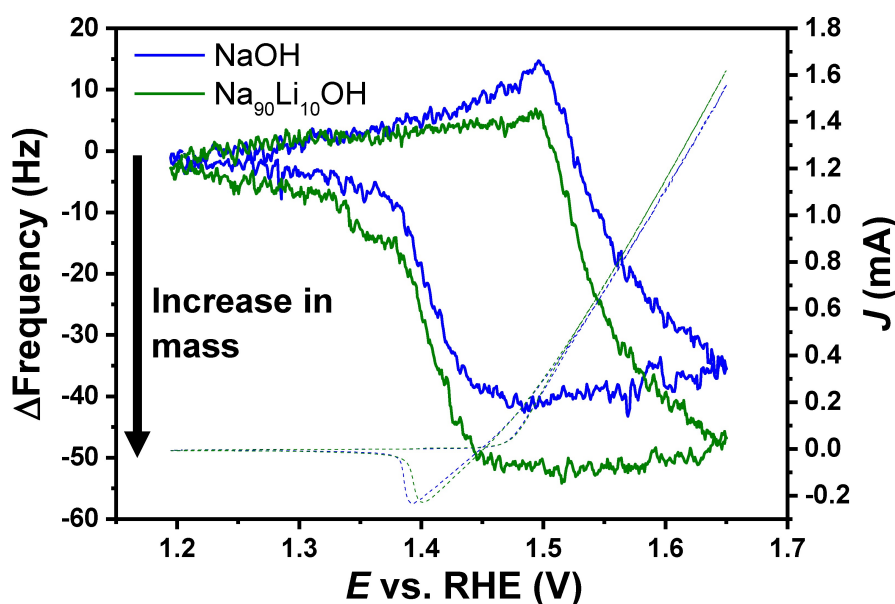


**Figure 3.** eQCM and CV in 0.1 M NaOH (blue) and  $\text{Na}_{90}\text{Li}_{10}\text{OH}$  (green), showing increased mass intercalation for the  $\text{Na}_{90}\text{Li}_{10}\text{OH}$  electrolyte. The potential has not been corrected for the ohmic drop.

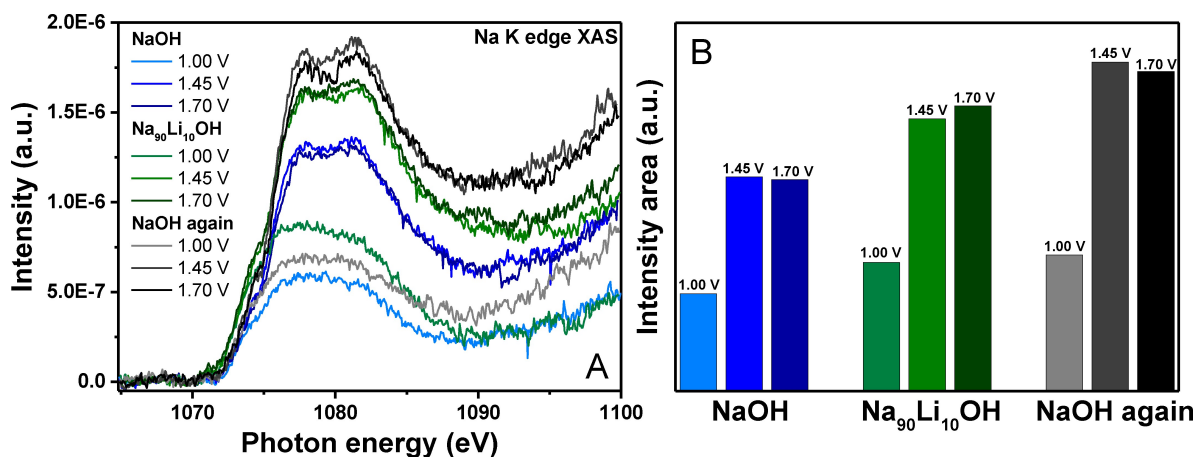


**Figure 4.** (A) Na K-edge spectra (absolute intensity) showing increased Na<sup>+</sup> intercalation with Na<sub>90</sub>Li<sub>10</sub>OH compared to pure NaOH. Changing the electrolyte back to 0.1 M NaOH shows even more Na<sup>+</sup>, indicating that this increased sodium uptake is caused by a (semi-)permanent change in the catalyst layer, (B) bar graphs of the integrated sodium XAS signal in the different electrolytes. The current recorded during these measurements are given in Figure S18.

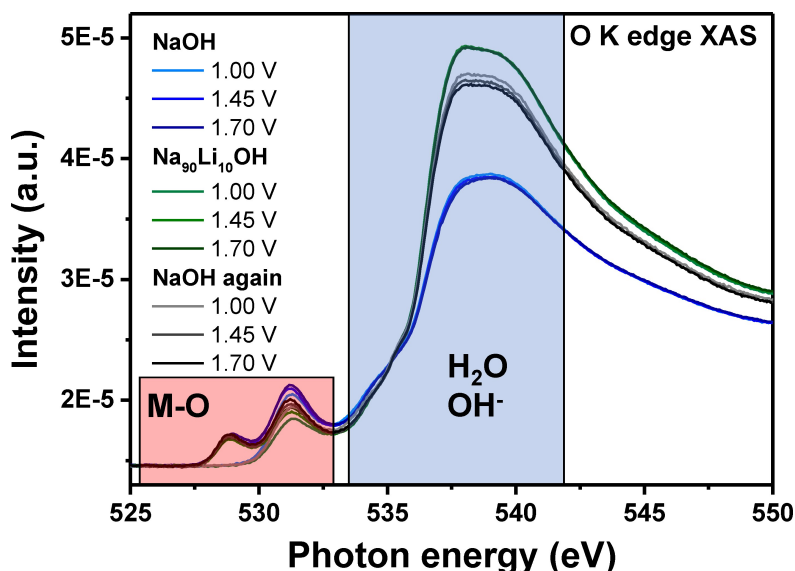


**Figure 5.** Oxygen K-edge spectra (absolute intensity), with more pronounced water/hydroxide intercalation with 10 mM LiOH in solution, as observed by the strongly increased signal intensity between 535 and 545 eV. The lattice oxygen species are shown and discussed in Figure S20.

This increase in water/hydroxide is not much dependent on applied potential, which could be another indication that the signal mostly comes from water. This shows that the addition of LiOH improves the electrolyte penetration into the porous catalyst layer, which can probably be related to the increased activity as shown in Figures 1 and 2. Here, again, the Li<sup>+</sup> effect is (semi-)permanent, as shown by the more pronounced H<sub>2</sub>O/OH<sup>-</sup> signal when the electrolyte was changed back to 0.1 M NaOH, where the H<sub>2</sub>O/OH<sup>-</sup> peak intensity is still considerably more pronounced than with the initial NaOH measurement. For the M–O species the intensity becomes lower with higher water and hydroxide intercalation. This can be explained as a result of the expansion of the metal oxide film due to the electrolyte penetration which equates to a smaller amount of metal-

oxide being present within the probing depth of the X-rays. That this effect is not caused by catalyst detachment was confirmed with the Ni L-edge as shown in Figure S19.

In Figure 6, the nickel L-edge spectra are shown for the different electrolytes. In the lower part of the figure, the references are provided for Ni in the 2+, 3+ or 4+ oxidation states. It can be observed that during and after using Na<sub>90</sub>Li<sub>10</sub>OH as electrolyte, there is a pronounced increase in the Ni<sup>4+</sup> peak at 1.7 V (not iR corrected) relative to Ni<sup>2+</sup>. We relate this to the higher accessibility of redox active sites with (and after) 0.1 M Na<sub>90</sub>Li<sub>10</sub>OH as the electrolyte, due to the improved electrolyte penetration as shown in Figures 3, 4 and 5. Again, it is observed that Li<sup>+</sup> can induce a (semi-)permanent change in the catalyst. To make sure that these changes between the electrolytes

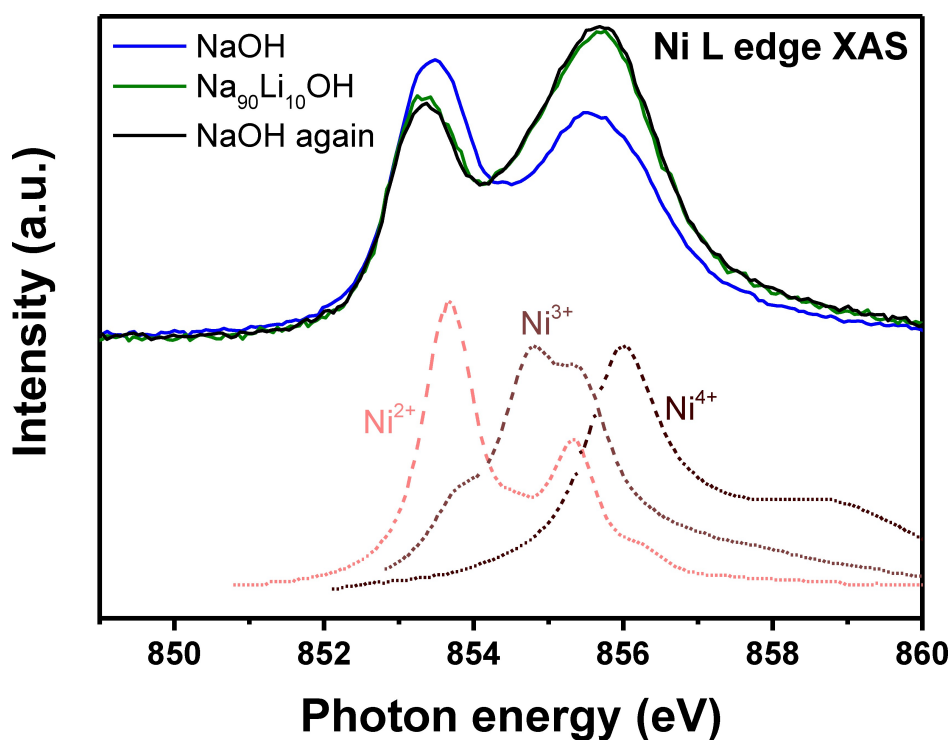


**Figure 6.** Ni L-edge XAS measurements (absolute intensity) at 1.7 V vs. RHE (not iR corrected) in NaOH,  $\text{Na}_{90}\text{Li}_{10}\text{OH}$  and NaOH again, below the reference spectra are given for Ni in 2+, 3+ or 4+ oxidation states.<sup>[23]</sup> More  $\text{Ni}^{4+}$  is observed with and after  $\text{Na}_{90}\text{Li}_{10}\text{OH}$ .

observed here did not occur as a result of catalyst detachment, the absolute intensities of the Ni spectra at 1.0 V were compared, and no significant degradation was observed during the XAS measurements (Figure S19). Similar to the increased Ni oxidation states, more reactive oxygen species<sup>[22]</sup> were observed in the O K-edge spectra when normalised to the lattice oxygen peak at 531.1 eV, which we again relate to the improved electrolyte accessibility (Figure S20).

To further confirm that the improved activity is due to improved transport in the catalyst layer, a catalyst with  $\sim 4\times$  lower mass loading was measured and compared, as a catalyst with very low loading should be much less limited by electrolyte penetration. On this layer the effect of LiOH promotion of the OER is much smaller, which is consistent with the  $\text{Li}^+$  activation being related to the electrolyte penetration (Figure 7). It can be observed that at low current density the differences in OER activity are negligible, but at increasing current density some slight OER

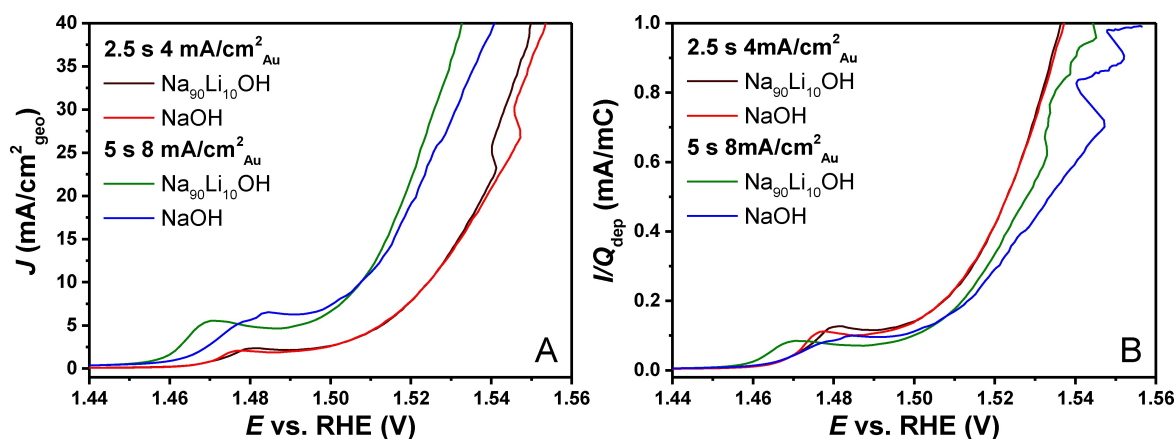


**Figure 7.** (A) LSVs of NiFeOOH layers with two different loadings, 2.5 s  $- 4 \text{ mA/cm}^2_{\text{Au}}$  and 5 s  $- 8 \text{ mA/cm}^2_{\text{Au}}$  in 0.1 M NaOH and  $\text{Na}_{90}\text{Li}_{10}\text{OH}$  at 2500 RPM, (B) LSV of the same experiment but with the current normalised to the charged passed during electrodeposition ( $Q_{\text{dep}}$ ), to estimate the specific current density.

promotion with  $\text{Li}^+$  in solution might still be observed. When the current density is normalised to the geometric current density, the low loading catalysts will already have a much higher specific current density at the same geometric current density. Therefore, in Figure 7B the current has been normalised to the total charge passed during the electrodeposition, which is related to the amount of deposited catalyst. Therein, it can be appreciated how at roughly similar specific current densities the  $\text{Li}^+$  activation effect is much more pronounced for higher loadings. For industrial applications, usually high loadings and high current densities ( $0.5\text{--}2\text{ A/cm}^2_{\text{geo}}$ ) are used, so improving transport within the catalyst layer will definitely be beneficial there.

With the nature of the  $\text{Li}^+$  activation clarified, it can now be seen in the context of the wider efforts to improve the diffusion through the interlayer spacing of the LDH materials. It is most likely that the interlayer distance of the LDH, here considered the “pore”, has to expand to accommodate the measured sodium, water and hydroxide, although a direct measurement of the interlayer distance has not been performed. Such efforts into improving interlayer diffusion are motivated by the observation that limited diffusion through LDH layers is detrimental for the electrochemical response of  $\text{NiOOH}^{[12]}$  and decrease the stability of the NiFe LDH at increasing current density.<sup>[24]</sup> The stability of bulkier NiFe LDH is worse due to decreasing local pH (more acidic), resulting in increased catalyst dissolution.<sup>[24]</sup> To mitigate the effects of  $\text{OH}^-$  transport limitations within the oxyhydroxide, efforts have been made to increase the interlayer distance of the LDH layers by intercalation of different anions,<sup>[2c, 25a]</sup> organics<sup>[25]</sup> or by the exfoliation of the layers.<sup>[26]</sup> However, most anions tend to be replaced by carbonate when exposed to  $\text{CO}_2$  in the air,<sup>[25b]</sup> and might not be very useful for application. Here, we have shown that mixed electrolytes containing  $\text{Li}^+$  in combination with other cations offer an alternative strategy.

Our observations may also shed light on the role of lithium in catalysts where lithium was incorporated during the synthesis. An example of this is Fe-substituted  $\text{LiNiO}_2$ , which has been reported to be an active OER catalyst.<sup>[27]</sup>  $\text{LiNiO}_2$  has recently been reported to be more active than  $\text{NiOOH}$ , and to become more active when Fe is added to the partially delithiated  $\text{LiNiO}_2$ .<sup>[28]</sup> The addition of Li during the catalyst synthesis has also been shown to increase the activities of  $(\text{Li})\text{CoFeO}_2$ <sup>[29]</sup> and  $(\text{Li})\text{IrOx}$ .<sup>[30]</sup> We may speculate that the in situ structure of these catalysts during OER operation is in fact quite similar to the one observed here, with the  $\text{Li}^+$  serving as a “pore-opener”. If that is correct, then similar results could be obtained for these materials by the addition of  $\text{Li}^+$  to the electrolyte instead of during the synthesis.  $\text{Li}^+$  as an additive in the anolyte could facilitate active site accessibility and therefore improve electrocatalyst performance, while avoiding issues with leaching.

More generally, our data shows that in mixed electrolytes, different cations can have different roles. While the details of the Li enhancement may require further research, we postulate that lithium acts as a pore-opener in NiFeOOH LDH. On the other hand, too much lithium adversely affects

the OER activity at the active sites (see Figures 1A and Figure S4). Hence, another cation is needed to serve as the main counter ion for the  $\text{OH}^-$  used in the reaction. As a result, an optimum is found for a low  $\text{Li}^+$  concentration in combination with larger quantities of  $\text{Na}^+$  or  $\text{K}^+$  (Figure S4). This concept of different ions cooperating to achieve optimal performance highlights the potential of mixed electrolytes in electrocatalysis and could be extended to a large range of catalysts and reactions.

## Conclusion

In conclusion, we have shown that the addition of small amounts of  $\text{Li}^+$  to Fe-free NaOH or KOH electrolytes, while keeping the pH constant, activates NiFeOOH for the oxygen evolution reaction (OER). This effect is robust and reproducible, under various synthesis and experimental conditions. The OER onset is similar and the initial Tafel slope value is  $30\text{ mV/dec}$  in both NaOH and  $\text{Na}_{90}\text{Li}_{10}\text{OH}$  electrolytes, showing no change in the kinetics or rate-determining step. However, the increase in apparent Tafel slope remains lower with increasing current density, which indicates that the activation is related to the mitigation of non-kinetic effects. eQCM and in situ XAS experiments demonstrated the origin of the  $\text{Li}^+$  activation effect by showing that more sodium, water and hydroxide are present in the porous catalyst layer when  $\text{Li}^+$  is present in the electrolyte. We propose that this superior electrolyte penetration into the porous catalyst layer results in an increased amount of accessible sites, which results in increased  $\text{Ni}^{4+}$  sites at relevant OER potentials. More generally, our work shows that cations can have different roles in mixed electrolytes:  $\text{Li}^+$  induces pore opening, but  $\text{Na}^+$  or  $\text{K}^+$  cations are still required for high activity. Importantly, the  $\text{Li}^+$  promotion effect becomes more pronounced for higher mass loading and at increasing current densities, which are relevant conditions for industrial electrolyzer systems. Our work shows how the specific tailoring of the electrolyte composition to the electrocatalyst can be an important strategy to optimize electrocatalytic performance.

## Acknowledgements

OvdH and MTMK gratefully acknowledge the funding provided by the Dutch Research Council (NWO) as part of the Reversible Large-scale Energy Storage (RELEASE) consortium (project number 17621). This work also received funding from the European Research Council (ERC), Advanced Grant no. 101019998 “FRUMKIN”. RVM and ND acknowledge the Dutch Research Council (NWO) for funding under grant number ECCM.TT.ECCM.001. HT acknowledges support from the German Federal Ministry of Education and Research in the framework of the project Catlab (03EW0015A/B). We acknowledge the Helmholtz-Zentrum Berlin (HZB) for providing access to the beamline U49-2\_PGM-1 at the synchrotron-radiation facility BESSY

II. We acknowledge Dr. Sipeng Zheng for performing the ICP-MS analysis.

### Conflict of Interest

The authors declare no conflict of interest.

### Data Availability Statement

The data that support the findings of this study are available from the corresponding author upon reasonable request.

**Keywords:** oxygen evolution reaction · cation effect · lithium · electrolyte · intercalation · XAS · eQCM

- [1] D. A. Corrigan, *J. Electrochem. Soc.* **1987**, *134*, 377–384.
- [2] a) S. Anantharaj, K. Karthick, S. Kundu, *Mater. Today Energy* **2017**, *6*, 1–26; b) F. Dionigi, P. Strasser, *Adv. Energy Mater.* **2016**, *6*, 1600621; c) B. M. Hunter, W. Hieringer, J. R. Winkler, H. B. Gray, A. M. Müller, *Energy Environ. Sci.* **2016**, *9*, 1734–1743; d) M. Wehrens-Dijksma, P. H. L. Notten, *Electrochim. Acta* **2006**, *51*, 3609–3621.
- [3] a) M. Gong, H. Dai, *Nano Res.* **2014**, *8*, 23–39; b) J. Mohammed-Ibrahim, *J. Power Sources* **2020**, *448*, 227375.
- [4] O. Diaz-Morales, D. Ferrus-Suspedra, M. T. M. Koper, *Chem. Sci.* **2016**, *7*, 2639–2645.
- [5] a) J. D. Michael, E. L. Demeter, S. M. Illes, Q. Fan, J. R. Boes, J. R. Kitchin, *J. Phys. Chem. C* **2015**, *119*, 11475–11481; b) L. Trotochaud, S. L. Young, J. K. Ranney, S. W. Boettcher, *J. Am. Chem. Soc.* **2014**, *136*, 6744–6753; c) R. Farhat, J. Dhainy, L. I. Halaoui, *ACS Catal.* **2020**, *10*, 20–35; d) D. Y. Chung, P. P. Lopes, P. F. B. D. Martins, H. He, T. Kawaguchi, P. Zapol, H. You, D. Tripkovic, D. Strmcnik, Y. Zhu, S. Seifert, S. Lee, V. R. Stamenkovic, N. M. Markovic, *Nat. Energy* **2020**, *5*, 222–230.
- [6] a) A. C. Garcia, T. Touzalin, C. Nieuwland, N. Perini, M. T. M. Koper, *Angew. Chemie - Int. Ed.* **2019**, *58*, 12999–13003; b) J. Huang, M. Li, M. J. Eslamibidgoli, M. Eikerling, A. Groß, *JACS Au* **2021**, *10*, 1752–1765.
- [7] S. Dresp, F. Dionigi, M. Klingenhof, T. Merzdorf, H. Schmies, J. Drnec, A. Poulain, P. Strasser, *ACS Catal.* **2021**, *11*, 6800–6809.
- [8] J. O. G. Posada, A. J. R. Rennie, S. P. Villar, V. L. Martins, J. Marinaccio, A. Barnes, C. F. Glover, D. A. Worsley, P. J. Hall, *Renew. Sustain. Energy Rev.* **2017**, *68*, 1174–1182.
- [9] a) D. M. Constantin, E. M. Rus, L. Oniciu, L. Ghergari, *J. Power Sources* **1998**, *74*, 188–197; b) D. Lei, D. C. Lee, A. Magasinski, E. Zhao, D. Steingart, G. Yushin, *ACS Appl. Mater. Interfaces* **2016**, *8*, 2088–2096.
- [10] E. M. Rus, D. M. Constantin, L. Oniciu, L. Ghergari, *Croat. Chem. Acta* **1999**, *72*, 25–41.
- [11] A. Mangel Raventos, R. Kortlever, *Electrochim. Acta* **2022**, *415*, 140255.
- [12] R. D. L. Smith, R. S. Sherbo, K. E. Dettelbach, C. P. Berlinguette, *Chem. Mater.* **2016**, *28*, 5635–5642.
- [13] P. Chakhranont, J. Kibsgaard, A. Gallo, J. Park, M. Mitani, D. Sokaras, T. Kroll, R. Sinclair, M. B. Mogensen, T. F. Jaramillo, *ACS Catal.* **2017**, *7*, 5399–5409.
- [14] a) F. Dionigi, Z. Zeng, I. Sinev, T. Merzdorf, S. Deshpande, M. B. Lopez, S. Kunze, I. Zegkinoglou, H. Sarodnik, D. Fan, A. Bergmann, J. Drnec, J. F. de Araujo, M. Gliech, D. Teschner, J. Zhu, W. X. Li, J. Greeley, B. Roldan Cuenya, P. Strasser, *Nat. Commun.* **2020**, *11*, 1–10; b) S. Z. Oener, A. Bergmann, B. Roldan Cuenya, *Nat. Synth.* **2023**, *2*, 817–827.
- [15] A. Bergmann, E. Martinez-Moreno, D. Teschner, P. Chernev, M. Gliech, J. F. de Araujo, T. Reier, H. Dau, P. Strasser, *Nat. Commun.* **2015**, *6*, 8625.
- [16] M. Görlin, J. H. Stenlid, S. Koroidov, H. Y. Wang, M. Börner, M. Shipilin, A. Kalinko, V. Murzin, O. V. Safonova, M. Nachtgeal, A. Uheida, J. Dutta, M. Bauer, A. Nilsson, O. Diaz-Morales, *Nat. Commun.* **2020**, *11*, 6181.
- [17] O. van der Heijden, S. Park, J. J. J. Eggebeen, M. T. M. Koper, *Angew. Chemie Int. Ed.* **2023**, *62*, e202216477.
- [18] M. T. M. Koper, *J. Solid State Electrochem.* **2023**.
- [19] P. Bernard, C. Gabrielli, M. Keddad, H. Takenouti, *Electrochim. Acta* **1991**, *36*, 743–746.
- [20] N. Shpigel, M. D. Levi, S. Sigalov, L. Daikhin, D. Aurbach, *Acc. Chem. Res.* **2018**, *51*, 69–79.
- [21] H. Trzesniowski, N. Deka, O. van der Heijden, R. Golnak, J. Xiao, M. T. M. Koper, R. Seidel, R. V. Mom, *J. Phys. Chem. Lett.* **2023**, *14*, 545–551.
- [22] a) V. Pfeifer, T. E. Jones, J. J. Velasco Vélez, R. Arrigo, S. Piccinin, M. Hävecker, A. Knop-Gericke, R. Schlögl, *Chem. Sci.* **2017**, *8*, 2143–2149; b) D. Drevon, M. Görlin, P. Chernev, L. Xi, H. Dau, K. M. Lange, *Sci. Rep.* **2019**, *9*, 1532; c) L. J. Frevel, R. Mom, J. J. Velasco-Vélez, M. Plodinec, A. Knop-Gericke, R. Schlögl, T. E. Jones, *J. Phys. Chem. C* **2019**, *123*, 9146–9152; d) V. Pfeifer, T. E. Jones, S. Wrabetz, C. Massué, J. J. Velasco Vélez, R. Arrigo, M. Scherzer, S. Piccinin, M. Hävecker, *Chem. Sci.* **2016**, *7*, 6791–6795.
- [23] R. Qiao, L. A. Wray, J. H. Kim, N. P. W. Pieczonka, S. J. Harris, W. Yang, *J. Phys. Chem. C* **2015**, *119*, 27228–27233.
- [24] R. Chen, S. F. Hung, D. Zhou, J. Gao, C. Yang, H. Tao, H. B. Yang, L. Zhang, L. Zhang, Q. Xiong, H. M. Chen, B. Liu, *Adv. Mater.* **2019**, *31*, 1903909.
- [25] a) L. Li, Y. Daib, Q. Xua, B. Zhanga, F. Zhanga, Y. Youa, D. Maa, S. S. Lia, Y. X. Zhang, *J. Alloys Compd.* **2021**, *882*, 160752; b) L. Huang, J. Jiang, L. Ai, *ACS Appl. Mater. Interfaces* **2017**, *9*, 7059–7067; c) L. Dang, H. Liang, J. Zhuo, B. K. Lamb, H. Sheng, Y. Yang, S. Jin, *Chem. Mater.* **2018**, *30*, 4321–4330; d) J. A. Carrasco, R. Sanchis-Gual, A. Seijas-Da Silva, G. Abellan, E. Coronado, *Chem. Mater.* **2019**, *31*, 6798–6807.
- [26] F. Song, X. Hu, *Nat. Commun.* **2014**, *5*, 4477.
- [27] K. Zhu, T. Wu, Y. Zhu, X. Li, M. Li, R. Lu, J. Wang, X. Zhu, W. Yang, *ACS Energy Lett.* **2017**, *2*, 1654–1660.
- [28] H. Huang, Y. C. Chang, Y. C. Huang, L. Li, A. C. Komarek, L. H. Tjeng, Y. Orikasa, C. W. Pao, T. S. Chan, J. M. Chen, S. C. Haw, J. Zhou, Y. Wang, H. J. Lin, C. T. Chen, C. L. Dong, C. Y. Kuo, J. Q. Wang, Z. Hu, L. Zhang, *Nat. Commun.* **2023**, *14*, 2112.
- [29] Y. Zhu, W. Zhou, Y. Chen, J. Yu, M. Liu, Z. Shao, *Adv. Mater.* **2015**, *27*, 7150–7155.
- [30] J. R. Esquiús, D. J. Morgan, G. A. Siller, D. Gianolio, M. Aramini, L. Lahn, O. Kasian, S. A. Kondrat, R. Schlögl, G. J. Hutchings, R. Arrigo, S. J. Freakley, *J. Am. Chem. Soc.* **2023**, *145*, 6398–6409.

Manuscript received: December 6, 2023

Accepted manuscript online: February 7, 2024

Version of record online: March 22, 2024